Inter-annual and decadal changes in tropospheric and stratospheric ozone

Ziemke[1,2], J. R., and S. Chandra[3]

[1]Goddard Earth and Sciences Technology and Research, Morgan State University, Baltimore, Maryland, USA.
[2]NASA Goddard Space Flight Center, Greenbelt, Maryland, USA.
[3]Goddard Earth Sciences and Technology, University of Maryland Baltimore County, Baltimore, Maryland, USA.

(Submitted to *Atmos. Chem. Phys. Disc.*, September 2011)

Abstract. Ozone data beginning October 2004 from the Aura Ozone Monitoring Instrument (OMI) and Aura Microwave Limb Sounder (MLS) are used to evaluate the accuracy of the Cloud Slicing technique in effort to develop long data records of tropospheric and stratospheric ozone and for studying their long-term changes. Using this technique, we have produced a 32-year (1979-2010) long record of tropospheric and stratospheric ozone from the combined Total Ozone Mapping Spectrometer (TOMS) and OMI. The analyses of these time series suggest that the quasi-biennial oscillation (QBO) is the dominant source of inter-annual variability of stratospheric ozone and is clearest in the Southern Hemisphere during the Aura time record with related inter-annual changes of 30-40 Dobson Units. Tropospheric ozone also indicates a QBO signal in the tropics with peak-to-peak changes varying from 2 to 7 DU. Decadal changes in global stratospheric ozone indicate a turnaround in ozone loss around mid-1990's with most of these changes occurring in the Northern Hemisphere from the subtropics to high latitudes. The trend results are generally consistent with the prediction of chemistry-climate models which include the reduction of ozone destroying substances beginning in the late 1980's mandated by the Montreal Protocol.

1. Introduction.

The measurement of tropospheric ozone from satellite remote sensing began with the studies by *Fishman and Larsen* [1987] and *Fishman et al.* [1990]. In those studies tropospheric column ozone (TCO) was derived by subtracting co-located stratospheric column ozone (SCO) from total column ozone. SCO was calculated from Stratospheric Aerosol and Gas Experiment (SAGE) ozone profile measurements while Total Ozone Mapping Spectrometer (TOMS) measurements were used for total column ozone. The method was named the tropospheric ozone residual (TOR) technique and was effective in

producing global maps of tropospheric ozone albeit limited primarily to a seasonal climatology because of sparse data sampling for SAGE. *Chandra et al.* [2003] used the greater spatial and temporal coverage of stratospheric ozone from the Upper Atmosphere Research Satellite (UARS) Microwave Limb Sounder (MLS) in combination with TOMS total ozone to improve monthly maps of TOR. More recently *Ziemke et al.* [2006] and *Schoeberl et al.* [2007] used two separate residual algorithms combining Aura Ozone Monitoring Instrument (OMI) and MLS measurements to produce global fields of TOR with improved temporal and spatial coverage beyond previous studies.

An alternative residual technique is the convective-cloud differential (CCD) method [*Ziemke et al.*, 1998] which uses total column ozone and SCO from the same satellite instrument. The CCD method is the most basic form of "cloud slicing" for measuring tropospheric and stratospheric ozone [e.g., *Ziemke et al.*, 2001, 2009, and references therein]. Gridded measurements from the CCD method are restricted to the tropics; however mid-to-high latitude measurements may be obtained with this method and are given generally as zonal averages over the Pacific. An advantage with the CCD method is that by using a single instrument the potential errors arising from residual differencing are largely alleviated. This is important for deriving a long record of TCO and SCO from several combined instruments.

The CCD technique takes advantage of the fact that UV-measuring instruments such as Total Ozone Mapping Spectrometer (TOMS), Global Ozone Monitoring Experiment (GOME), and OMI do not measure ozone lying below optically thick clouds. The CCD method assumes that one can make an accurate estimate of SCO using high-reflecting deep convective clouds (reflectivity R>0.8) in the tropical Pacific region. It was shown by *Ziemke et al.* [2009] from combined Aura OMI and MLS measurements that ozone concentrations inside thick clouds in the Pacific are small to within a few ppbv. The CCD method works well for deriving SCO in the Pacific because the above-cloud column ozone measured by OMI for thick clouds is essentially equivalent to SCO to within 1-2 DU. The CCD method of *Ziemke et al.* [1998] further assumes that SCO is invariant along longitude in the tropics. With these assumptions, TCO in tropical latitudes can be calculated at any given location by differencing low reflectivity (R<0.2) total column ozone and high reflectivity (R>0.8) SCO from the Pacific region within the same latitude range. High reflecting clouds generally do not have physical cloud heights reaching tropopause altitude and the column ozone above the cloud may vary considerably even when R>0.8. As a practical solution, SCO in the Pacific is calculated using only minimum values of above-cloud column ozone in each gridded region. These minimum values are then averaged over the eastern and western tropical Pacific to derive a single measurement of SCO.

The validity of these assumptions has been established by comparing TCO and SCO derived from the CCD method with TCO and SCO derived from ozonesondes and satellite data including TOMS/MLS, TOMS/Halogen Occultation Experiment instrument (HALOE), and TOMS/SAGE combinations [e.g., *Ziemke et al.*, 1998, 2005; *Chandra et al.*, 2003]. Application of the CCD method from TOMS data was extended over the

Pacific region into the middle and high latitudes between 50°S and 60°N [*Ziemke et al.*, 2005] for the time record 1979-2003.

The objective of this study is to evaluate strengths and weaknesses of the CCD technique by incorporating Aura OMI and MLS ozone and to study inter-annual and decadal changes in tropospheric and stratospheric ozone. The Aura MLS measurements of SCO provide a stringent test of CCD SCO when compared to sparse satellite occultation measurements in previous studies. This is important for establishing a long record (1979-present) of CCD TCO and SCO from combined OMI and TOMS instrument measurements. Long record data products are important for addressing issues including trends in tropospheric ozone and pollution, stratospheric ozone depletion, and decadal changes in the global Brewer Dobson Circulation.

In the following, section 2 discusses the Aura OMI and MLS measurements, section 3 describes the CCD and OMI/MLS residual methodologies, section 4 discusses inter-annual variability of tropospheric and stratospheric ozone, section 5 discusses some results from the TOMS+OMI 1979-2010 extended ozone dataset, and finally section 6 provides a summary.

2. Aura OMI and MLS Ozone Measurements.

The OMI and MLS are two out of a total of four instruments onboard the Aura spacecraft which is flown in a sun-synchronous polar orbit at 705 km altitude with a 98.2° inclination. Aura was launched in July 2004 and has been providing data measurements since August 2004 to the present. The spacecraft has an equatorial crossing time of 1:45 pm (ascending node) with around 98.8 minutes per orbit (14.6 orbits per day on average). *Schoeberl et al.* [2006] provide an overview of the EOS Aura mission and discuss the various measurements from the four Aura instruments.

The OMI is a nadir-scanner which at visible (350-500 nm) and UV wavelength channels (UV-1: 270-314 nm; UV-2: 306-380 nm) detects backscattered solar radiance to measure column ozone with near global coverage (aside from polar night latitudes) over the Earth with a resolution of 13 km × 24 km at absolute nadir. Aside from ozone, OMI also measures Optical Centroid Cloud Pressure (OCCP), aerosols, NO_2, SO_2, HCHO, and several other trace gases in the troposphere and stratosphere [*Levelt et al.*, 2006]. Measurements of ozone from OMI are determined using the OMTO3 v8.5 algorithm which is an extension of the TOMS v8 algorithm. A description of the TOMS v8 algorithm may be obtained from the TOMS V8 CD DVD ROM, or from the OMI Algorithm Theoretical Basis Document (ATBD) from the TOMS web page http://toms.gsfc.nasa.gov/version8/v8toms_atbd.pdf). One difference between the TOMS v8 and the OMTO3 v8.5 algorithms is the treatment of clouds. The TOMS v8 and earlier versions of OMTO3 use a cloud pressure climatology based on thermal infrared cloud-top pressures, whereas OMTO3 v8.5 uses in situ OCCP derived with OMI by the rotational Raman scattering method.

SCO is calculated for the OMI/MLS residual method using MLS v2.2 ozone. The MLS instrument is a thermal-emission microwave limb sounder that measures vertical profiles of mesospheric, stratospheric, and upper tropospheric temperature, ozone, and several other constituents from limb scans taken in the direction ahead of the Aura satellite orbital track. The MLS profile measurements are made about 7 minutes before OMI views the same location during ascending (daytime) orbital tracks. These we refer to as "co-located" measurements between OMI and MLS. MLS also measures ozone and other atmospheric constituents for descending nighttime orbits which on a given day can be up to ±12 hours different in time from OMI daytime measurements. With combined ascending and descending nodes MLS makes around 3500 vertical profile measurements over the Earth per day. This study includes only the ascending orbit co-located data from MLS for deriving SCO. Details regarding the instrument including spectrometers, spectral channels, calibration, and other topics are discussed by *Waters et al.* [2006] and in related papers in the same journal. *Froidevaux et al.* [2008; and personal communication, 2011] provides validation results for MLS v2.2 measurements of ozone and other trace gases. At the present time an MLS v3.3 data product is also provided to the science community. While v2.2 retrieval has 37 pressure levels, v3.3 has 55 pressure levels and other improvements; however, v3.3 also has more outliers/missing data in the ozone measurements than with v2.2. Our analysis of SCO derived from MLS shows that there is little difference between using v2.2 or v3.3 other than a small systematic offset (v3.3 minus v2.2) of about 2.5 DU. Information regarding MLS v3.3 ozone measurements is available online from the NASA Data and Information Services Center (http://disc.sci.gsfc.nasa.gov/gesNews/mls_new_data_version_release).

3. The CCD and OMI/MLS Residual Methodologies.

Two residual methods are used for deriving TCO and SCO from Aura OMI and MLS measurements. The first is the approach of *Ziemke et al.* [2006] and the second is the CCD method of *Ziemke et al.* [1998]. Figure 1 is a schematic diagram illustrating both of these residual techniques in the tropics where the tropopause is typically ~16-17 km altitude year-round.

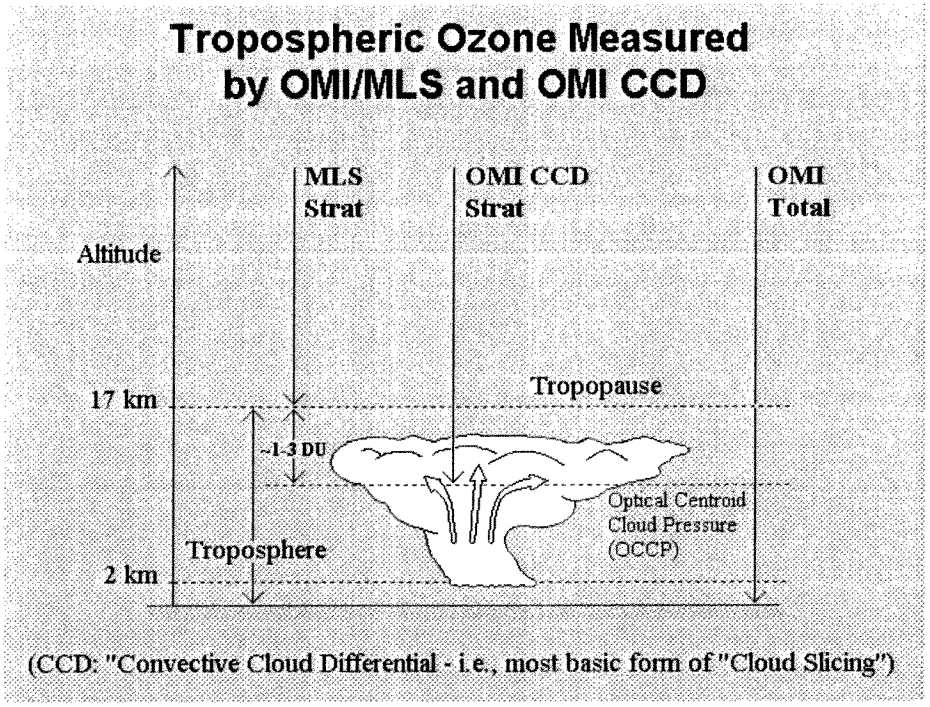

Figure 1. Schematic illustration of the OMI/MLS tropospheric ozone residual method (OMI total column ozone minus MLS stratospheric column ozone) and the convective-cloud differential (CCD) residual method (OMI total column ozone minus OMI above-cloud column ozone).

3.1. The OMI/MLS Residual Method.

For the OMI/MLS residual method in Figure 1, SCO is derived from vertically integrated MLS ozone profiles which are subtracted from OMI total column ozone to derive TCO. Tropopause pressure, which separates tropospheric from stratospheric column ozone comes from National Centers for Environmental Prediction (NCEP) using the World Meteorological Organization (WMO) 2K-km^{-1} lapse rate tropopause definition. SCO from MLS is determined by pressure integration of ozone volume mixing ratio profiles from 0.0215 hPa down to the NCEP tropopause. The MLS ozone profile measurements were linearly interpolated in log-pressure to the existing NCEP tropopause pressure to derive SCO. MLS SCO (in Dobson Units, DU; 1 DU = 2.69×10^{20} molecules-m^{-2}) was determined by standard log-pressure integration of ozone volume mixing ratio: $SCO = 0.79\int_{0.0215hPa}^{Ptropopause} XP \cdot d\ln P$, where X is ozone volume mixing ratio in units ppbv and P is pressure in units hPa. The recommended range for scientific analysis of MLS v2.2 ozone profiles is 0.0215-215 hPa. As was done by *Ziemke et al.* [2006], nearly global SCO from MLS for each day was achieved by including ozone retrievals down to 316 hPa.

MLS SCO data were binned to 1° latitude × 1.25° longitude to be compatible with OMI level-3 (L3) gridded total column ozone. Tropopause pressures from NCEP analyses

were re-binned to this same resolution from a coarser 2.5° × 2.5° gridding. It is noted for MLS limb measurements that the horizontal optical path is about 300 km which is larger than the horizontal size of OMI L3 gridded data, but is comparable to the size of original NCEP gridded measurements. To derive a high density SCO field we have used the two-step spatial interpolation of *Ziemke et al.* [2006]. The interpolation for SCO includes first a moving 2D (latitude/longitude) Gaussian window along daytime orbit to fill in intermittent gaps along-track for MLS SCO, followed secondly by a linear interpolation along longitude between existing MLS SCO data. This interpolation approach preserves the along-track measurements of SCO from MLS at all latitudes. NCEP measurements of tropopause pressure were re-binned to the same 1° latitude × 1.25° longitude resolution. Following the determination of SCO and TCO at 1° × 1.25° resolution, the SCO data were averaged in 5° × 5° bins to be compatible with OMI SCO from the CCD method.

3.2. The CCD Residual Method.

The CCD method illustrated in Figure 1 uses a collective ensemble of high reflectivity (i.e., reflectivity R>0.8) above-cloud column ozone measurements from OMI within specified gridded regions (here 5° latitude × 5° longitude boxes) to determine SCO. Cloud tops that lie lower in the troposphere will have larger above-cloud column ozone amounts provided that spatial variability of ozone is small over the region. High reflectivity scenes represent generally deep convective cloud systems, however their physical cloud tops may not generally reach tropopause altitude and column ozone above the cloud may vary considerably even with R>0.8. As a practical approach, SCO in the Pacific is estimated statistically within each gridded region using only minimum values of above-cloud column ozone. This is done within each region by subtracting 2σ from the mean value where σ is calculated RMS of the ensemble. All calculations are made each day with an absolute minimum number of R>0.8 level-2 footprint scenes in each 5° × 5° region chosen as 10.

The minimum ensemble values are associated with deep convective clouds with small ozone concentration lying between the OCCP and the tropopause. Evidence for the latter effect in tropical latitudes was shown by *Kley et al.* [1996] during the Central Equatorial Pacific Experiment (CEPEX). Their study indicated from ozonesondes near-zero ozone concentrations in the upper troposphere with the passing of deep convective cloud systems. Possible mechanisms stated for the exceedingly low ozone measurements in the upper troposphere included chemical destruction of ozone by yet unidentified reactions and vertical transport via convective clouds of very low ozone concentrations from the low troposphere. Low ozonesonde concentration in the upper troposphere is also described in later studies by *Folkins et al.* [2002] and *Solomon et al.* [2005] as an indicator of deep convection and associated vertical injection of low ozone amounts upwards from the boundary layer/low troposphere. *Vomel and Diaz* [2010] in a more recent paper suggest that the near-zero ozone concentrations in the upper troposphere by *Kley et al.* [1996] were biased low because of uncertainties in ozonesonde cell currents. Following a reprocessing of the CEPEX ozonesondes, *Vomel and Diaz* [2010] indicated that lowest ozonesonde concentrations in the upper troposphere in the Pacific may be more typically ~10 ppbv. Assuming a constant mixing ratio of 10 ppbv lying between

the tropopause and OMI OCCP (~300-500 hPa for minimum above-cloud ozone scenes) this is equivalent to 1-3 DU in column amount. Even with such non-zero ozone concentrations lying between the tropopause and OCCP for thick clouds, the estimate of SCO in the Pacific from the CCD method should still be accurate to about 1-3 DU in absolute numbers.

3.2.1. Comparisons of CCD and OMI/MLS Gridded Tropical TCO measurements

The primary measurement derived from the CCD method of *Ziemke et al.* [1998] is gridded TCO in low tropical latitudes. We have evaluated the CCD TCO data from OMI by comparing with coincident OMI/MLS residual measurements. Figure 2 shows TCO from the CCD method (left panels) with TCO from OMI/MLS (right panels) for four consecutive October months beginning in 2004. It is well known that October (like September and November) coincide each year with large enhancements of tropospheric ozone in the tropical south Atlantic. This zonal wave-one pattern in TCO in the tropics is caused largely by a combination of effects from the dynamical Walker circulation and photochemical sources including biomass burning and lightning [e.g., *Sauvage et al.*, 2007, and references therein].

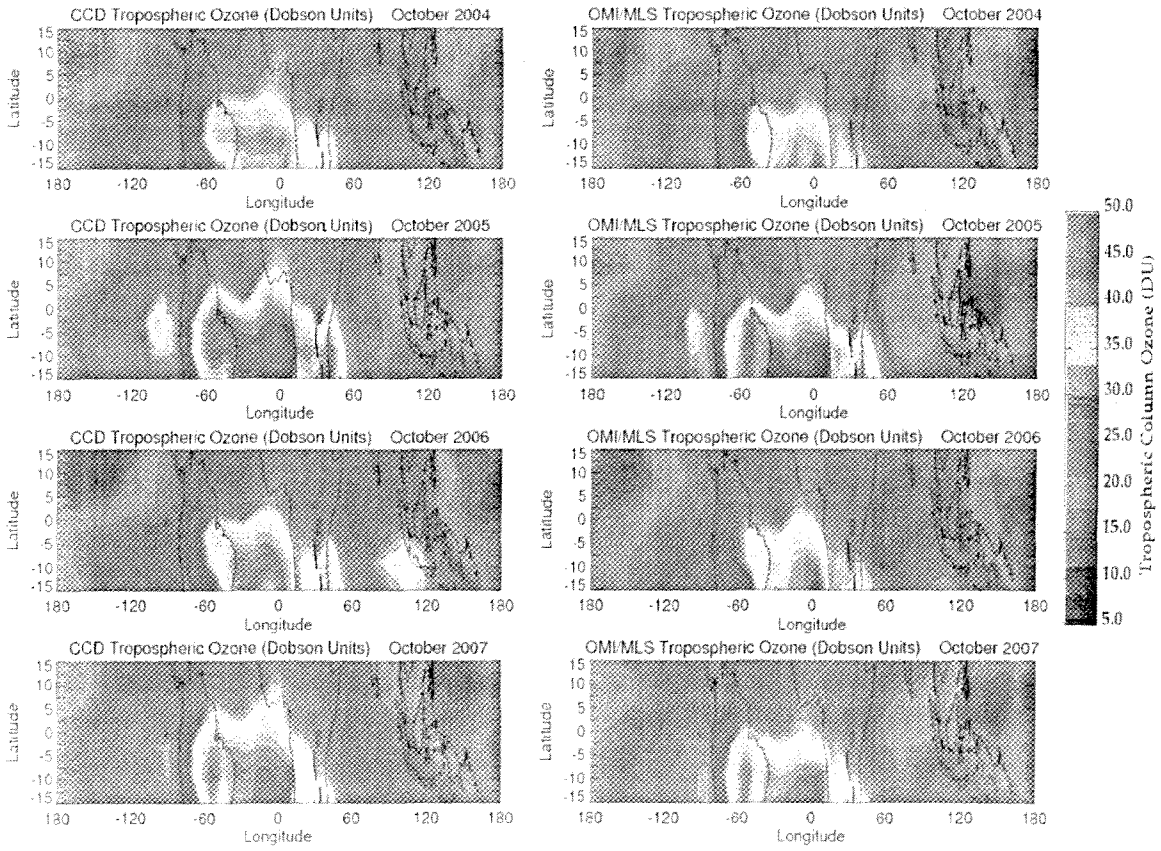

Figure 2. Tropospheric column ozone (in Dobson Units) derived from the CCD residual method (left panels) and the OMI/MLS residual method (right panels) for four

consecutive October months beginning in 2004. Blue to red colors represent smallest to largest values, respectively.

There is substantial inter-annual variability present in Figure 2 in the Atlantic region where year-to-year differences are ~10 DU. October 2004 and 2006 coincided with two El Nino events whereas October 2005 was non-ENSO (i.e., neither El Nino nor La Lina conditions) and October 2007 coincided with a strong La Nina event. Although ENSO events are predominantly an Indian Ocean/Pacific Ocean phenomenon, it is possible that ENSO may have contributed in some way to the observed ozone inter-annual variability in the Atlantic where lowest ozone abundance is seen to occur during El Nino events. It is also possible that unrelated year-to-year changes in ozone precursors and/or meteorological conditions is the primary cause for the inter-annual variations in Atlantic TCO. There is also evidence as discussed later in section 5.1 of reduction of tropical tropospheric ozone in years 2004 and 2006 related to the quasi-biennial oscillation (QBO). (The analysis of inter-annual variability of TCO in the Atlantic is beyond the scope of this study.)

Figure 3 shows a scatter plot comparing the two TCO products accumulated over the entire six years in the tropical domain 15°S-15°N (as shown in Figure 2). The ensemble averages and RMS values listed in Figure 3 are comparable for the two products with average values of about 27 DU and 6 DU, respectively. The calculated RMS of CCD minus OMI/MLS difference time series is much smaller at around 3 DU with an overall cross-correlation between the two datasets of 0.88. The conclusion from Figures 2 and 3 is that these two gridded products are essentially similar with an average of about 3 DU statistical RMS difference and nearly zero offset.

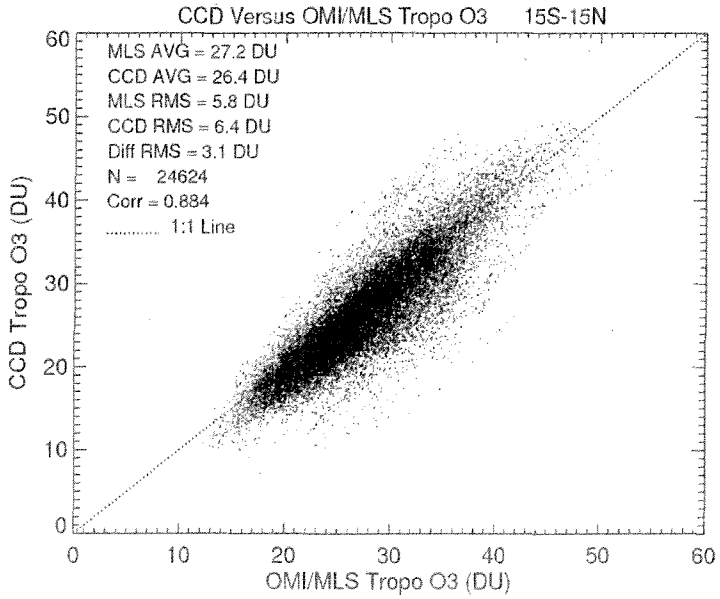

Figure 3. Scatter plot of CCD versus OMI/MLS monthly mean gridded tropospheric column ozone (in Dobson Units) accumulated over the six-year record in the tropics. The measurements for both products are gridded at 5°×5° latitude-longitude resolution and extend from central latitudes 12.5°S to 12.5°N along all longitudes

3.2.2. Tropospheric Ozone Associated with Deep Convective Clouds.

Key to the CCD method is the abundance of ozone lying inside deep convective clouds. Figure 4 shows seasonal contour plots of the difference of OMI CCD minimum above-cloud column ozone minus MLS SCO averaged over the six years. We refer to these residual differences in Figure 4 as "cloud ozone" which represents tropospheric column ozone lying between the tropopause and OCCP under conditions of deep convective clouds (i.e., scenes where reflectivity exceeds 0.8). It is inferred that much of the column ozone amounts shown in Figure 4 are a manifestation of ozone lying in the boundary layer/lower troposphere that is injected upward into these clouds. Some of the measurements in Figure 4 are negative and even exceed -5 DU in high latitudes, particularly during winter months. The negative column amounts in Figure 4 are obviously not correct and are caused by yet unresolved offset differences between MLS SCO and OMI above-cloud column ozone in wintertime high latitudes where solar zenith angles are highest, often exceeding 75°.

Ideally, wherever the CCD method is working correctly in deriving local measurements of SCO the differences between the two ozone datasets in Figure 4 should be zero. The differences in Figure 4 are generally small in the Pacific extending from the tropics to high latitudes, but there are offset differences as large as 10 DU or even 20 DU in the extra-tropics of both hemispheres in regions away from the Pacific. It will be shown that these offset differences are mostly recurring annual cycle features and that tropospheric and stratospheric ozone from the CCD method are more accurate after these measurements are deseasonalized.

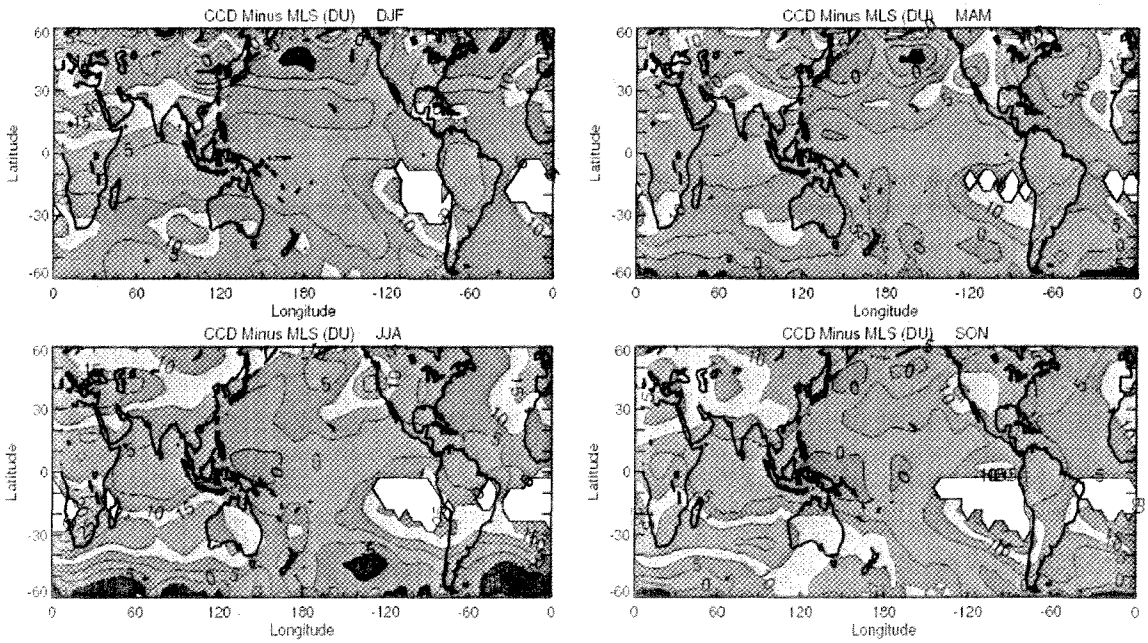

Figure 4. Three-month seasonal averages (December-February, March-May, June-August, and September-November) of CCD above-cloud column ozone minus MLS stratospheric column ozone over the time record 2004-2010. Contour numbers represent

Dobson Units. The colors violet/blue to orange represent negative to positive values, respectively. We denote these measurements in this figure as "cloud ozone", the amount of column ozone lying between the tropopause and cloud OCCP under conditions of deep convection.

Line plots of 12-month annual cycles of CCD cloud ozone in the Pacific in 20° latitude bands from 60°S to 60°N are shown as solid curves in Figure 5. Plotted also as dotted curves in Figure 5 are corresponding TCO time series from OMI/MLS. We refer to these measurements as background "ambient" ozone. Included in Figure 5 for all time series are calculated standard error of mean numbers which provide a measurement proportional to inter-annual variability; as example, inter-annual variability for cloud ozone in high latitudes in Figure 5 is around 3-4 time larger than in the tropics.

The annual cycles and annual mean values for cloud ozone measurements in the tropics in Figure 5 are small at only about 1-3 DU, however annual cycles and annual means can exceed 5 DU in the extra-tropics. Ambient ozone in Figure 5 maximizes in spring-summer months (March-July) in the Northern Hemisphere and the spring months (September-November) in the Southern Hemisphere. The cloud ozone in Figure 5 is always substantially smaller than ambient ozone at all latitude ranges, yet within the RMS uncertainties the annual cycles are generally similar for both column amounts.

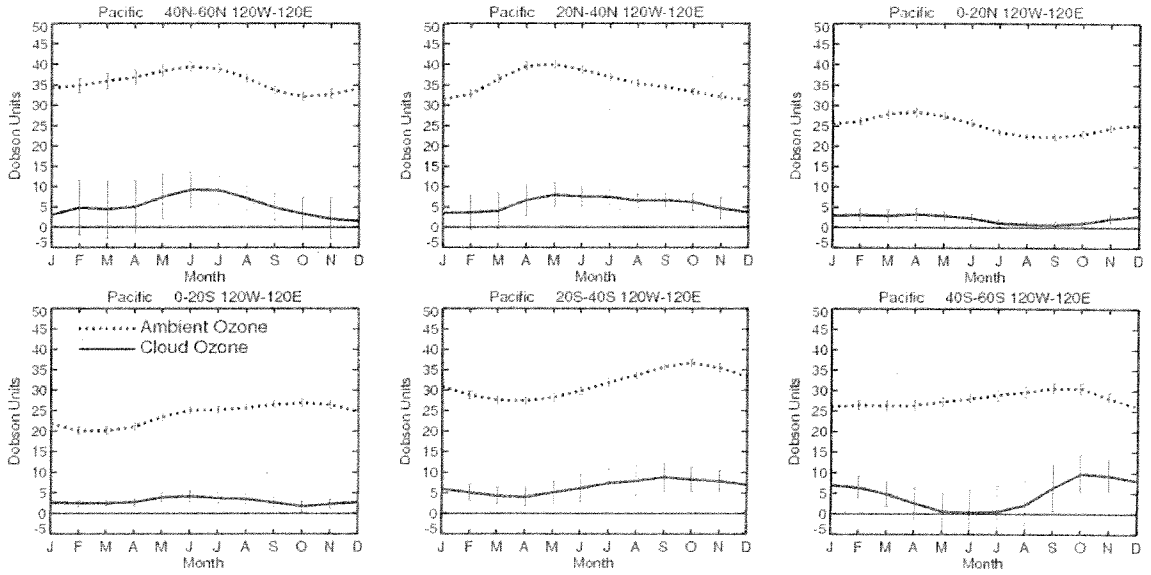

Figure 5. Solid curves: Line plots of CCD 12-month annual cycles of cloud ozone averaged within six non-overlapping 20° latitude bands in the Pacific. The latitude bands are (from upper left to lower right): 40°N-60°N, 20°N-40°N, 0°-20°N, 0°-20°S, 20°S-40°S, and 40°S-60°S. The Pacific averaging is for the longitude domain 120°W-120°E about the dateline. Dotted curves: Same as solid curves but for background ambient column ozone from OMI/MLS residual. These annual cycle time series are all derived by averaging together data for similar months over the six years. The vertical bars represent calculated ±1σ RMS standard error of mean.

Figure 6 is the same as Figure 5 except that the time series were derived for zonal means rather than Pacific means. The conclusions for zonal means are similar to those discussed for Pacific means except that cloud ozone annual means are larger at most latitudes for zonal mean measurements. Figure 7 shows more annual cycle line plot comparisons, but instead for six extra-tropical regions where cloud ozone often exceeds 5-20 DU (i.e., exceeding 50% of ambient ozone in some months). It is interpreted that these extra-tropical regions are more polluted with boundary layer/lower tropospheric ozone. The annual cycles for cloud ozone and ambient ozone are not correlated for Southeast Asia and southern Africa in Figure 7. For southern Africa, ambient ozone maximizes in September-October (same as the other two Southern Hemisphere regions in the figure), whereas cloud ozone maximizes much earlier around August; August is a peak month for biomass burning in the southern Africa region.

The conclusions from Figures 4-7 are that Pacific means and zonal means have nearly the same geophysical signatures in annual cycles for both the cloud ozone and ambient ozone, and also that most of the offset differences in Figure 4 (which represent ozone measured in deep convective clouds) are recurring annual cycle features. Later in section 4 we will show that after removing annual cycles from the data that inter-annual variability for the Pacific mean and zonal mean data products of both TCO and SCO from the CCD method are precise measurements to within a few DU relative to OMI/MLS residual ozone, not just in the tropics but extending to high latitudes.

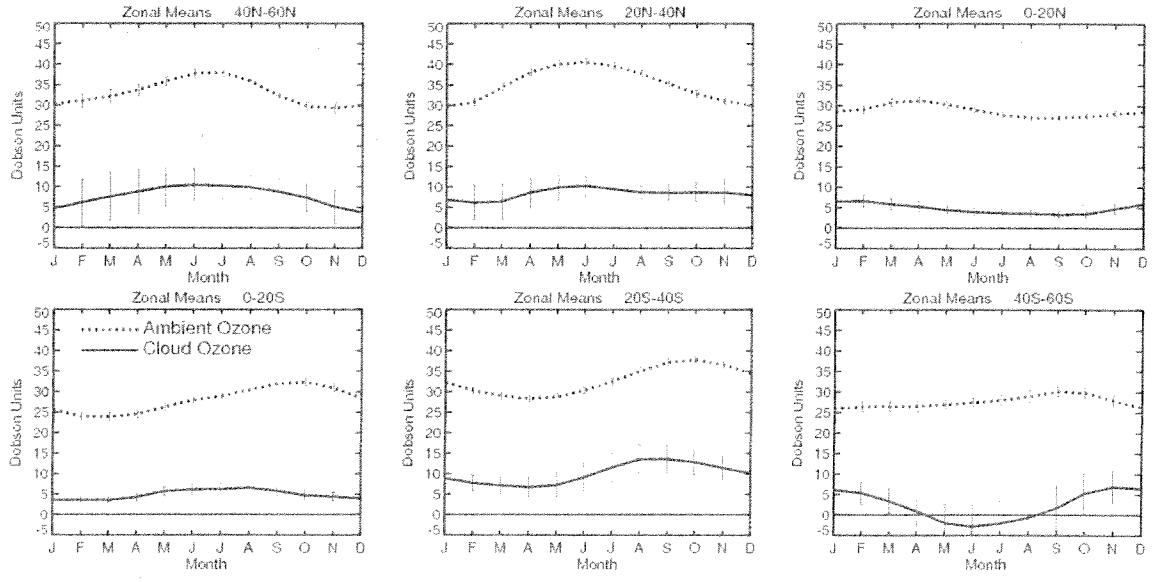

Figure 6. Similar to Figure 5 but for zonal mean measurements.

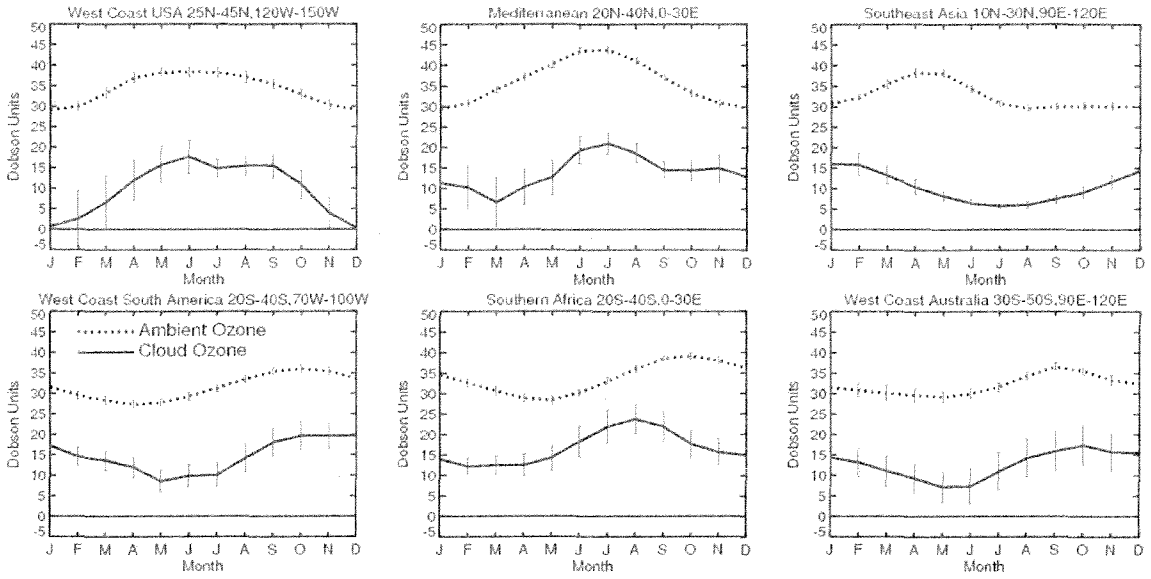

Figure 7. Similar to Figures 5 and 6 but instead for six broad regions of the globe where measured CCD cloud ozone is large with peak abundances of ~15-20 DU. These six regions are from upper left to lower right (compare these regions with Figure 4): West Coast of the USA, Mediterranean, Southeast Asia, West Coast of South America, Southern Africa, and West Coast of Australia.

4. Inter-annual Variability of Tropospheric and Stratospheric Ozone.

In the study by *Ziemke et al.* [2005] the CCD measurements of TCO and SCO from combined Nimbus 7 and Earth Probe TOMS were extended to middle and high latitudes in the Pacific under the assumption that deep convective clouds with low boundary layer ozone conditions persist outside the tropics just as they do in the tropics. The CCD measurements of SCO were tested against SAGE II SCO for the time period 1984-2003. Despite sparse SAGE measurements those comparisons showed that SAGE and CCD SCO in the extra-tropics compared well in annual means and even better (to 2-4 DU differences) from the tropics to high latitudes when comparisons were made for summer months only.

We use the Aura MLS measurements of SCO which have greater spatial and temporal coverage than SAGE to evaluate how well the CCD method works outside tropical latitudes. Figure 8 compares latitude versus month contour diagrams of SCO averaged over the Pacific (120°W-120°E) from OMI CCD (top) and MLS (bottom). SCO in middle and high latitudes for either OMI or MLS in Figure 8 is largest in both hemispheres from winter into spring with large 80-100 DU peak-to-peak annual-cycle changes. There is indication of large inter-annual variability in both data sets from the tropics to high latitudes which includes an apparent QBO signal in the tropics with a period of about two years.

The SCO data in Figure 8 were further deseasonalized to evaluate inter-annual changes (Figure 9). Deseasonalization was accomplished by subtracting for each month a global monthly mean climatology value (determined by averaging similar months over the six-

year record). The dominant inter-annual signature in Figure 9 is the QBO which during the Aura record shown has about a 24-month period and is characteristically centered about the equator extending to high latitudes of both hemispheres.

The tropically driven QBO induces a global secondary circulation with opposite vertical wind fields between the tropics and extra-tropics [e.g., *Andrews et al.*, 1987]. Subsidence (ascent) of stratospheric air mass in equatorial latitudes associated with the QBO-induced circulation coincides with ascent (subsidence) of stratospheric air mass in the extra-tropics. In the tropics the subsidence of air mass driven by the QBO during the descending westerly phase (i.e., descending eastward zonal winds in the low-mid stratosphere) is seen in Figure 9 as anomalous increases in tropical SCO that maximize around the months May-October for years 2006 and 2008. The QBO-induced down-welling circulation in the tropics coincides with opposite upwelling in the extra-tropics which is seen in Figure 9 as anomalous reductions in SCO of 10-20 DU in high latitudes of both hemispheres in winter-spring months. The extra-tropical QBO variability appears clearer in the Southern Hemisphere because of a synchronous phase coupling between the Brewer Dobson Circulation annual component and the QBO which during the Aura record had about a 24-month cycle.

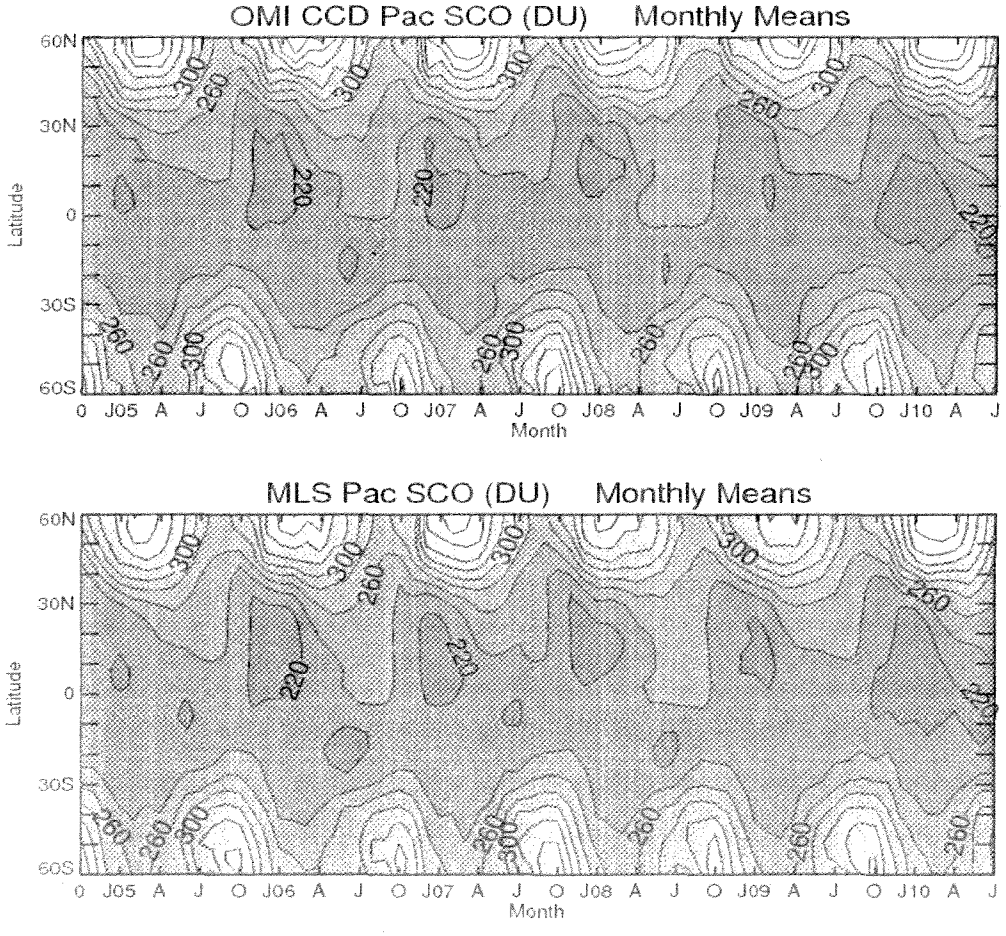

Figure 8. Latitude versus month contour diagrams of monthly mean stratospheric column ozone (in Dobson Units) averaged over the Pacific (120°W-120°E) from OMI CCD (top) and MLS (bottom). Dark to light shading designates smaller to higher column amounts, respectively. The contour values for both diagrams begin at 200 Dobson units and increment by 20 Dobson Units.

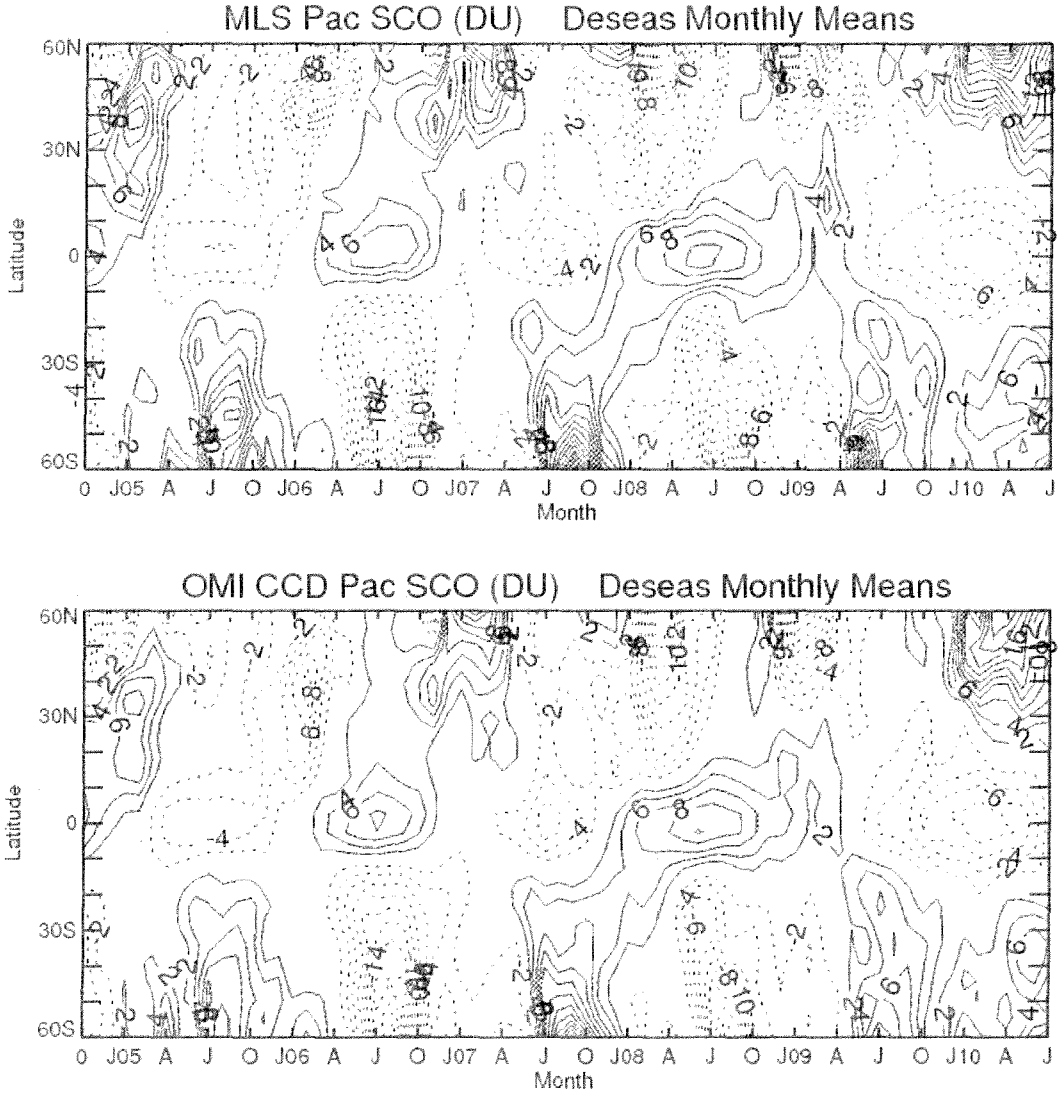

Figure 9. Contour diagrams of the same stratospheric column ozone (in Dobson Units) plotted in Figure 8, but instead with all of the data deseasonalized.

Toward the end of the record in Figure 9 there is anomalously large SCO in the northern higher latitudes beginning around January 2010 for both OMI and MLS. These increases coincide with ozone decreases in the tropics associated with the descending easterly phase of the QBO. A recent study by *Steinbrecht et al.* [2011] combined ozonesondes from Hohenpeissenberg (48°N, 11°E) and SCIAMACHY total ozone to conclude that

450 these high values of ozone in 2010 were among the largest on record in northern latitudes
451 during the last 20-25 years. Their study attributes these large ozone enhancements to a
452 coupling between the QBO and the Arctic Oscillation and North Atlantic Oscillation with
453 the latter two oscillations being in an unusually persistent negative phase.
454
455 Time series of SCO corresponding to the data in Figures 8 and 9 are plotted in Figure 10
456 in 10° latitude bands (indicated) for monthly means (left panels) and deseasonalized
457 monthly means (right panels). Shown in all panels in Figure 10 are Pacific averages for
458 CCD (solid curves) and MLS (dotted curves). Despite seasonally varying offsets up to 5-
459 10 DU between CCD and MLS in the left panels in Figure 10, when the data are
460 deseasonalized the month-to-month differences between the two ozone datasets is
461 reduced for all latitude ranges. The deseasonalized time series in Figure 10 for both
462 residual methods show that the QBO-related signal in the Southern Hemisphere high
463 latitudes is associated with inter-annual changes of ~30 DU or greater.
464

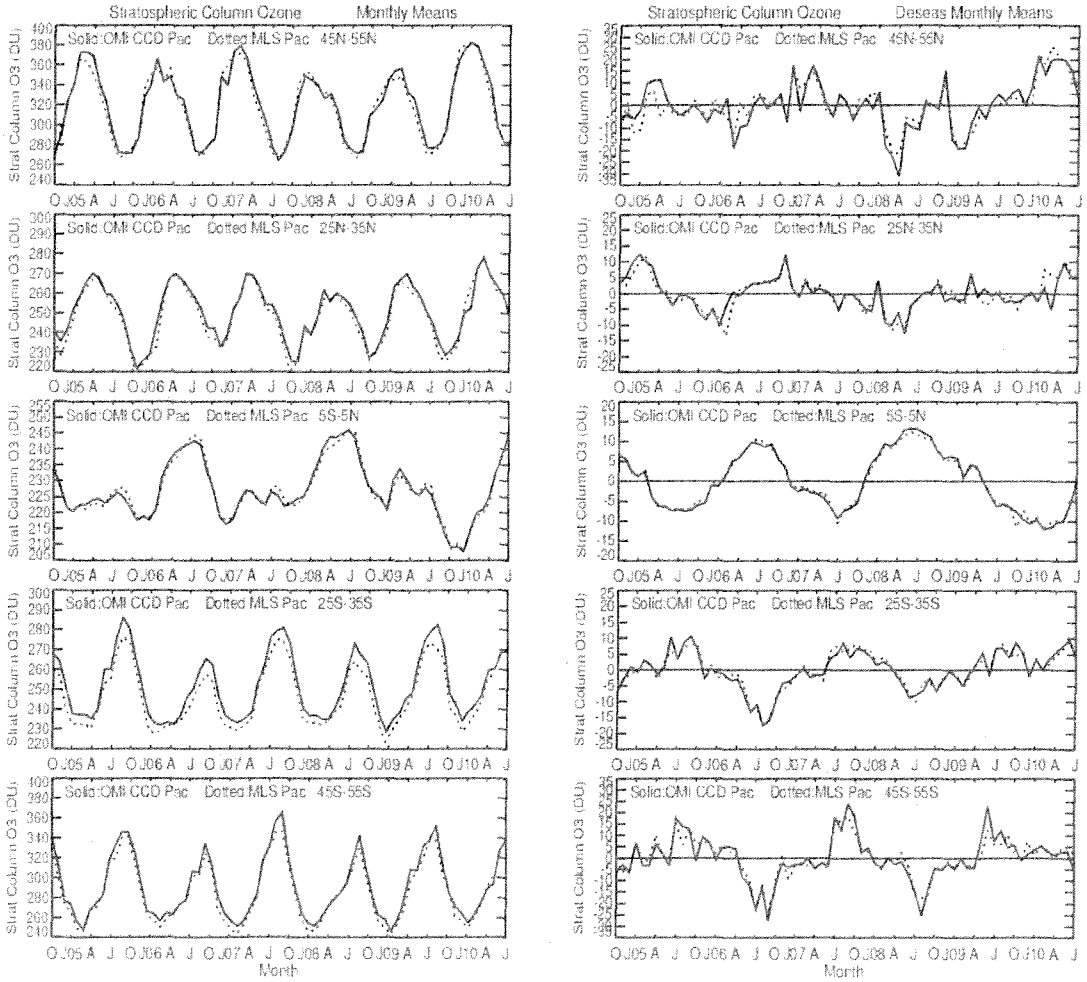

465
466 **Figure 10.** (Left panels) Monthly averaged Pacific mean measurements of CCD SCO
467 from OMI (solid curve) and MLS SCO (dotted curve) averaged over five indicated 10°
468 latitude bands. The Pacific mean represents data averaged over the combined eastern and
469 western Pacific (i.e., longitude range 120°W to 120°E about the dateline). All

measurements are in Dobson Units. (Right panels) Same as left panels but with the data deseasonalized.

Pacific mean tropospheric ozone derived from the two residual methods is shown in Figure 11. Figure 11 is the same as Figure 10 but with TCO plotted rather than SCO. Shown in Figure 11 are the original time series (left panels) and deseasonalized time series (right panels) for the same five latitude bands. There are obvious offset differences between the two methods in the left panels in Figure 11 which are up to ~10 DU in some months. The deseasonalized TCO time series in the right panels do not have these offsets and track each other reasonably well.

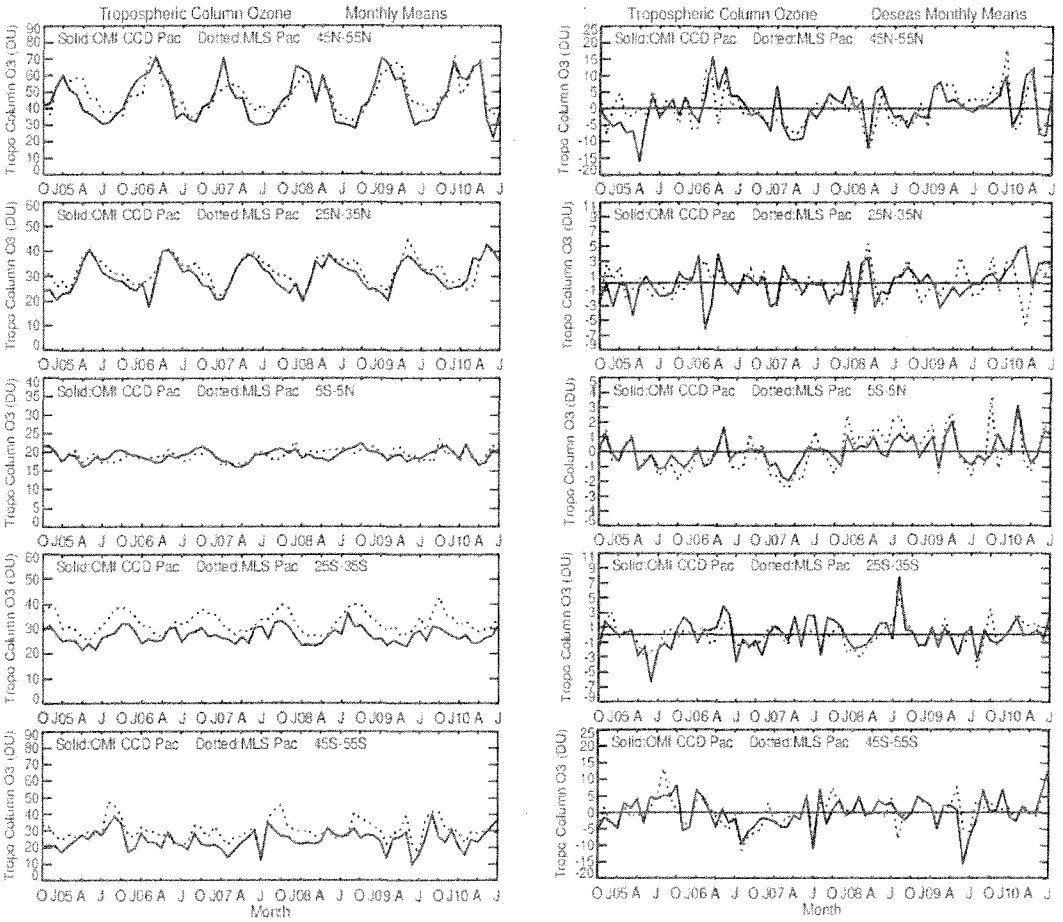

Figure 11. (Left panels) Monthly averaged Pacific mean measurements of CCD TCO from OMI (solid curves) and OMI/MLS TCO (dotted curves) averaged over five indicated 10° latitude bands. The Pacific mean represents data averaged over the combined eastern and western Pacific (i.e., longitude range 120°W to 120°E about the dateline). All measurements are in Dobson Units. (Right panels) Same as left panels but with the data deaseasonalized.

Figures 9-11 suggest that inter-annual variability of Pacific mean SCO and TCO from the CCD method from the tropics to high latitudes compares closely to within a few DU with corresponding measurements from the OMI/MLS residual method. We will show that

zonally averaged CCD above-cloud column ozone also compares close to zonal mean SCO from MLS.

Figure 12 shows contour diagrams of deseasonalized zonal mean SCO from MLS (top panel) and OMI CCD above-cloud column ozone (bottom panel). Comparison with Figure 9 suggests that SCO from the two methods are closer for zonal means than for Pacific means.

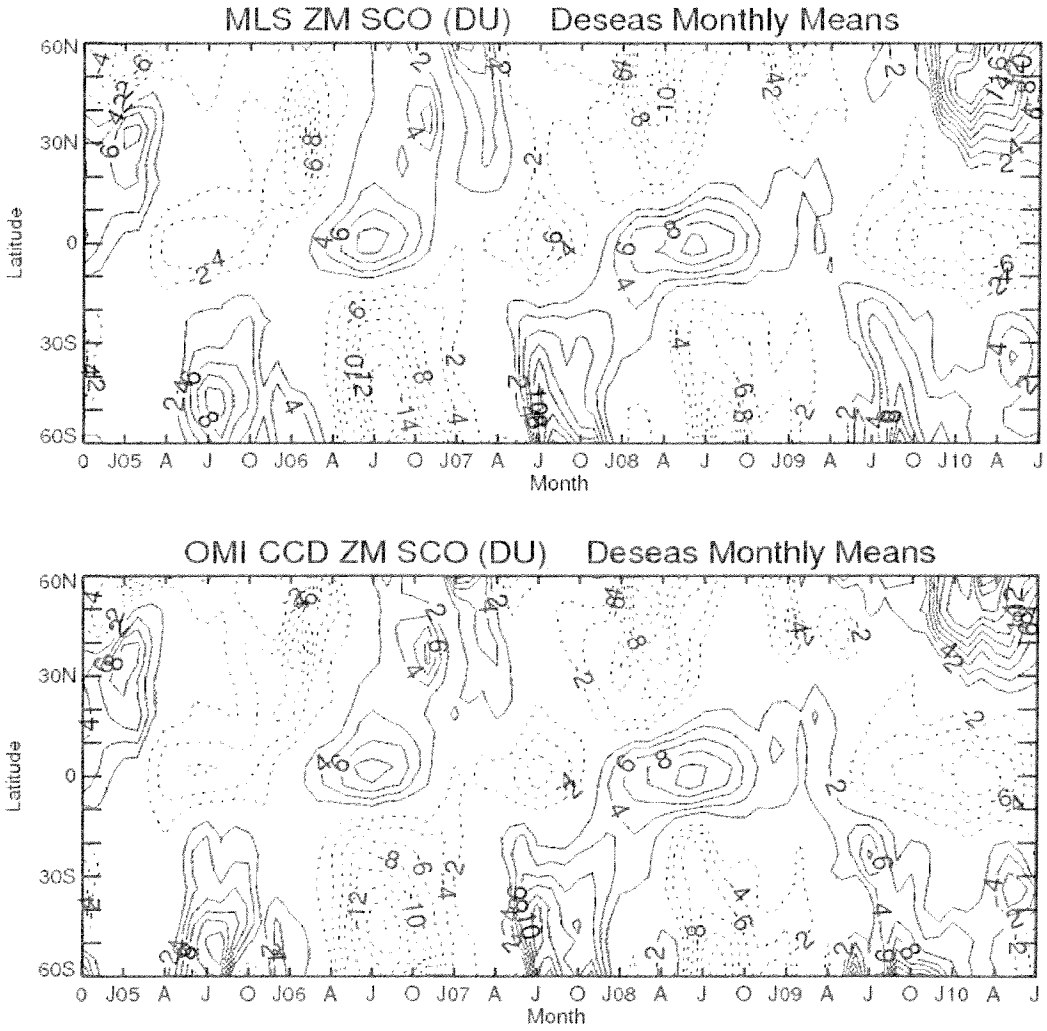

Figure 12. Same as Figure 9, but instead for zonal means rather than Pacific means.

Figure 13 plots temporal RMS values of the difference between CCD and MLS deseasonalized SCO time series for Pacific means (asterisks) and zonal means (triangles) as a function of latitude. (The RMS amplitudes for Pacific means and zonal means in Figure 13 were calculated from OMI minus MLS differences of the data plotted in Figures 9 and 12, respectively.) The RMS values in Figure 13 for most latitudes are generally about 1-2 DU and up to ~2-3 DU at higher latitudes. For zonal means RMS differences are about 0.5-1 DU in the tropics to ~1.5 DU at mid-to-high latitudes. The RMS values in Figure 13 for SCO are equivalent to RMS amplitudes calculated for TCO.

This is because the same OMI total column ozone measurements are used for both residual methods.

These Aura comparisons have given us greater confidence in the CCD measurements of tropospheric and stratospheric ozone derived from previous TOMS measurements. In the next section we discuss a long record of stratospheric and tropospheric ozone determined from combined TOMS and OMI records beginning 1979.

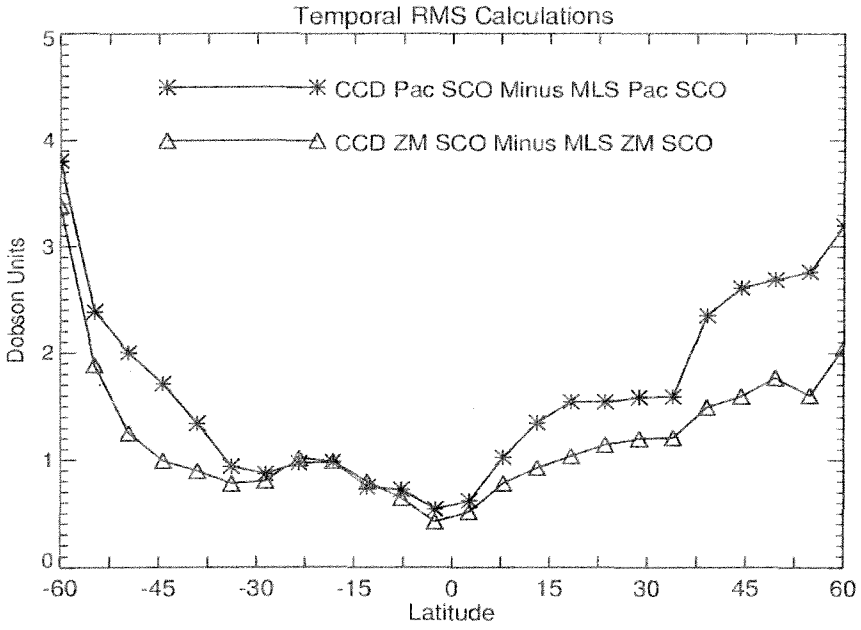

Figure 13. Calculated temporal RMS values (in Dobson Units) of the difference between CCD and MLS deseasonalized SCO time series for Pacific means (asterisks) and zonal means (triangles) as a function of latitude. These RMS amplitudes were calculated from the difference between the data plotted in Figures 9 and 12, respectively.

5. The TOMS+OMI Ozone Dataset.

We have developed an extended record of tropospheric and stratospheric column ozone spanning 1979-2010 by combining TOMS and OMI Pacific mean CCD measurements. It was noted in the data description section that the TOMS ozone uses the version 8 algorithm while OMI ozone uses the version 8.5 algorithm. Although there may be retrieval offsets existing between TOMS and OMI measurements because of different algorithms for the separate instruments, our analyses suggest that these offsets are not large and cannot be more than a few DU at most at any latitude. Offsets of only a few DU will adversely affect evaluation of inter-annual variability and calculated trends in tropospheric ozone, but such offsets have less relative impact for stratospheric ozone. In the near future we plan to combine the TOMS and OMI stratospheric and tropospheric ozone data using only the single version 9 processed retrievals. We provide only a brief discussion of ozone trends and inter-annual (QBO) variability in tropospheric ozone for the 1979-2010 data record.

5.1. Quasi-Biennial Oscillation Signals in Tropical Ozone.

Although it is well known that there exists a large QBO variability in stratospheric ozone, there is also evidence of a QBO in tropospheric ozone. *Ziemke and Chandra* [1999] first detected a possible QBO in tropospheric ozone using Nimbus-7 TOMS measurements for the 1979-1993 record. A later study by *Chandra et al.* [2002] combined Nimbus-7 TOMS with Earth Probe TOMS and found a consistent QBO in tropospheric ozone over a longer record of 1979-2000. The QBO in tropospheric ozone for these studies was clearer to detect in the Atlantic region as opposed to the Pacific as there is additional inter-annual variability in the Pacific related to ENSO events. It was postulated by *Ziemke and Chandra* [1999] that a possible source for the QBO signal could be an upper tropospheric ozone photochemistry response from the QBO in stratospheric ozone. However, the measured tropospheric signal was larger than predicted by photochemical models and it was concluded by *Ziemke and Chandra* [1999] that the source for the QBO signal in tropospheric ozone was most likely of dynamical origin. *Lee et al.* [2010] have reached these same conclusions based upon balloon sonde data from the Southern Hemisphere Additional Ozonesondes (SHADOZ) network. Their analyses of the sonde temperature and ozone measurements suggest that the QBO signal in tropospheric ozone extends down to about mid-troposphere and is of dynamical origin.

Figure 14 plots 50 hPa monthly zonal winds from Singapore (1°N, 104°E) (dotted curve) and deseasonalized tropospheric ozone (solid curve) averaged in the equatorial Atlantic (5°S-5°N, 60°W-60°E). There are two data gaps present in the time series in Figure 14. The first gap is several years of non-existing measurements between Nimbus 7 and Earth Probe TOMS periods. The second gap in Figure 14 represents Earth Probe CCD measurements which have been conservatively flagged as missing after year 2000 for questionable data quality. Tropospheric ozone in Figure 14 was additionally smoothed using a low-pass digital filter as described in the figure caption.

Comparison of the 50 hPa zonal winds and tropospheric ozone in Figure 14 indicates a persistent negative correlative relationship over the long 32-year multi-instrument record. The QBO signal in tropospheric ozone for the 1979-1993 Nimbus-7 TOMS period in Figure 14 is larger than during the latter EP TOMS and OMI periods. Peak-to-peak differences in ozone for the Nimbus-7 record are ~4-7 DU compared to ~2-4 DU for the latter years. There are some years in Figure 14 where the wind/ozone negative correlation relation is not evident. One case occurs around 1990-1991 (coinciding with the July 1991 Mt. Pinatubo eruption), and another case is in 1997-1998 during an intense tropical El Nino event.

We conclude from the TOMS+OMI 32-year record that there appears to be a persistent QBO signal in tropospheric ozone with peak-to-peak amplitudes varying from about 2 DU up to 7 DU. This evidence further strengthens claims from previous studies of a QBO in tropospheric ozone. We note that *Lee et al.* [2010] from ozonesonde analyses found maximum QBO signal in tropospheric ozone profile measurements of about 8 ppbv (equivalent to ~2-3 DU in upper troposphere) which is not inconsistent with the signal amplitudes that we find from the TOMS+OMI combined record.

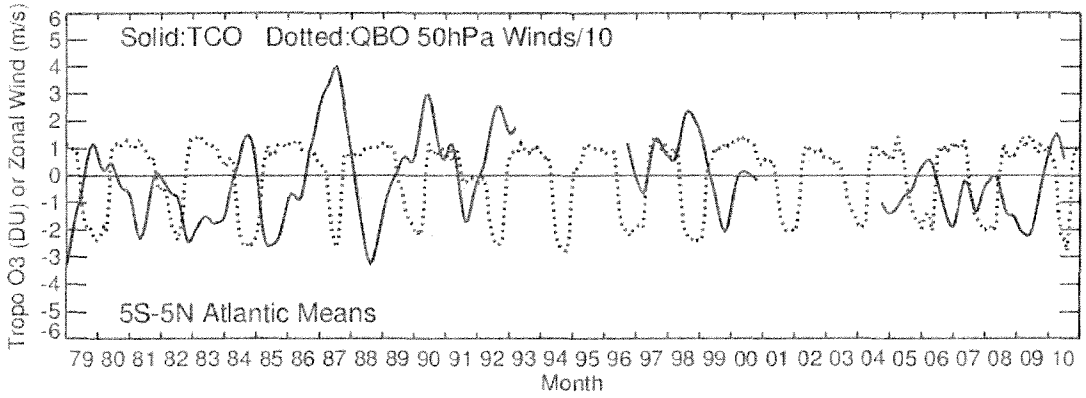

Figure 14. Tropospheric column ozone from the CCD method in Dobson Units (solid curve) plotted versus 50 hPa zonal winds from Singapore (1°N, 104°E) in units m-s^{-1} but divided by 10 for scaling (dotted curve). The ozone time series was averaged over the equatorial Altantic region (5°S-5°N, 60°W-60°E). The ozone time series was deseasonalized and detrended, and then smoothed using a recursive low-pass digital filter with one-half filter response at 12-month period (filter response of about 0.8-0.9 for 24-36 month QBO time periods).

5.2. Ozone Trends.

Trends in tropospheric and stratospheric ozone were calculated by *Ziemke et al.* [2005] for a 25-year record (1979-2003) of TOMS CCD measurements in the Pacific. It was shown that stratospheric ozone trends for the Pacific are nearly identical to trends calculated for zonal means. *Ziemke et al.* [2005] found that trends in tropospheric ozone were near zero most everywhere but marginally positive (~+2 DU to +3 DU decade^{-1}) in mid-latitudes of both hemispheres. Trends in stratospheric column ozone were also near zero in the tropics but large and negative (~ -10 to -14 DU decade^{-1}) in the mid-high latitudes of both hemispheres. We have made similar calculations of trends using the extended TOMS+OMI 32-year record. The results presented are limited to stratospheric ozone trends; tropospheric ozone trends for the 32-year record are not substantially different from trends shown by *Ziemke et al.* [2005] based on 25 years of data.

Figure 15 shows calculated trends in Pacific-averaged stratospheric ozone for the TOMS+OMI 32-year record (solid curve) and also, as comparison, stratospheric ozone trends for the Nimbus-7 15-year record beginning from 1979 (dotted curve). The trends in Figure 15 were calculated using the seasonally varying multivariate regression model of *Ziemke et al.* [2005] which included regression fits for combined linear trend, seasonal cycle, QBO, Solar cycle, and ENSO. It is apparent in Figure 15 that the negative trends in stratospheric ozone outside the tropics have reduced in magnitude markedly over the long record compared to the early 15-year record. The largest reduction in trends lies in the Northern Hemisphere extending from the subtropics to high latitudes. Area weighting of the trend differences in Figure 15 for latitudes 50°S to 50°N indicates that 66% of trend reduction lies in the Northern Hemisphere. Trends of 10 to 20 DU decade^{-1}

622 in the mid-high latitudes in Figure 15 correspond to trends of approximately 3 to 6%
623 decade^{-1}, respectively.
624

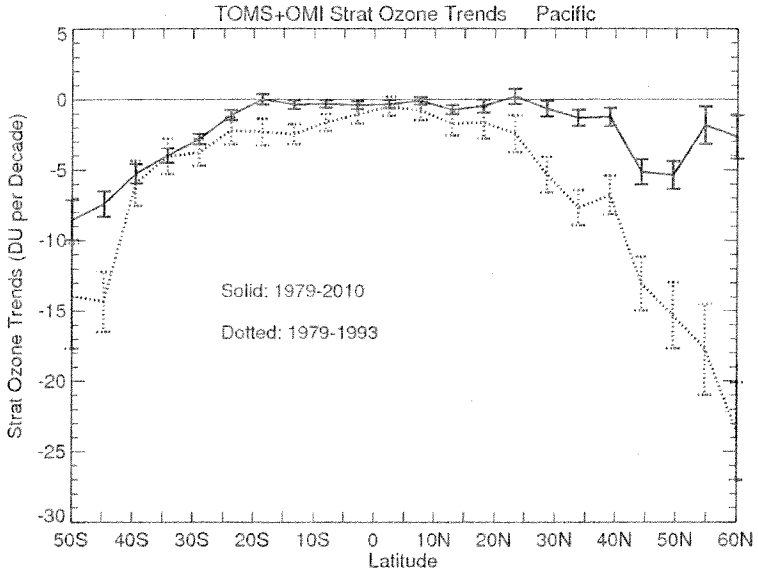

625
626 **Figure 15.** Trends (units DU decade^{-1}) in stratospheric column ozone for the extended
627 TOMS 1979-1993 CCD measurements derived from a linear multivariate regression
628 model (see text). (right) Same as left panel except for 1979-2010 extended TOMS+OMI
629 record. All data were averaged over the Pacific (120°W to 120°E about dateline) within
630 5° latitude bands. Vertical bars indicate ±2σ annual mean trend uncertainties calculated
631 from the regression model. The trend units and latitude range in this figure were chosen
632 to coincide with the trend figures shown by *Ziemke et al.* [2005] in which there were too
633 few Nimbus 7 CCD monthly measurements poleward of 50°S for seasonal trend analysis.
634
635 A complicating factor in assessing global stratospheric ozone recovery and turnaround
636 period of stratospheric ozone loss is solar cycle variability. Figure 16 (left panel) shows
637 annual mean time series of CCD stratospheric ozone (stars) plotted with merged total
638 column ozone from the NASA merged ozone webpage http://acdb-
639 ext.gsfc.nasa.gov/Data_services/merged/. The two time series represent column ozone
640 area averaged between 60°S and 60°N. For stratospheric ozone a constant 31 DU was
641 added to the time series for plotting with total column ozone. This 31 DU represents
642 mean global abundance of tropospheric ozone. Along the bottom in Figure 16 as a proxy
643 of solar UV variability is solar F10.7 cm radio flux time series [e.g., *Jackman et al.*, 1996,
644 and references therein].
645
646 One cannot readily identify a turnaround period in the ozone time records in the left panel
647 of Figure 16 because of a dominant solar cycle present. In the right panel of Figure 16
648 we have removed solar cycle variability in both ozone time series using regression
649 (discussed in figure caption). With solar variability removed we identify a turnaround
650 period occurring in the mid-1990's for stratospheric and total column ozone. We can
651 also conclude from the right panel in Figure 16 that tropospheric ozone does not indicate
652 substantial decadal changes.
653

The first paper to evaluate global ozone trends and recovery turnaround in models and satellite measurements was by *Jackman et al.* [1996] which used a 2D chemical transport model. Interestingly, their model predicted a turnaround in the mid-1990's and recovery of ozone by 2010 similar to the amounts present in the mid-1980's. These features are both present in the measurements in the right panel of Figure 16. Similar figures comparing total column ozone from models and measurements have been shown recently in the 2010 WMO report and by *Oman et al.* [2010, and references therein]. Most of these recent models predict a turnaround occurring around year 2000 with largely varying recovery time periods. Several of these models predict a longer ozone recovery to mid-1980's levels by year 2020 or later.

The Montreal Protocol was an international treaty initiated in 1987 to reduce worldwide ozone destroying substances such as chlorofluorocarbons and Bromine compounds. As a result of this treaty, since 1989 there has been a dramatic global reduction in these substances and a turnaround in ozone trends. Our 32-year ozone record indicates a turnaround in stratospheric ozone loss in the mid-1990's with recent ozone levels comparable to amounts present in the mid-1980's. These measurements seem to suggest a faster stratospheric ozone recovery occurring than predicted by many of the recent models.

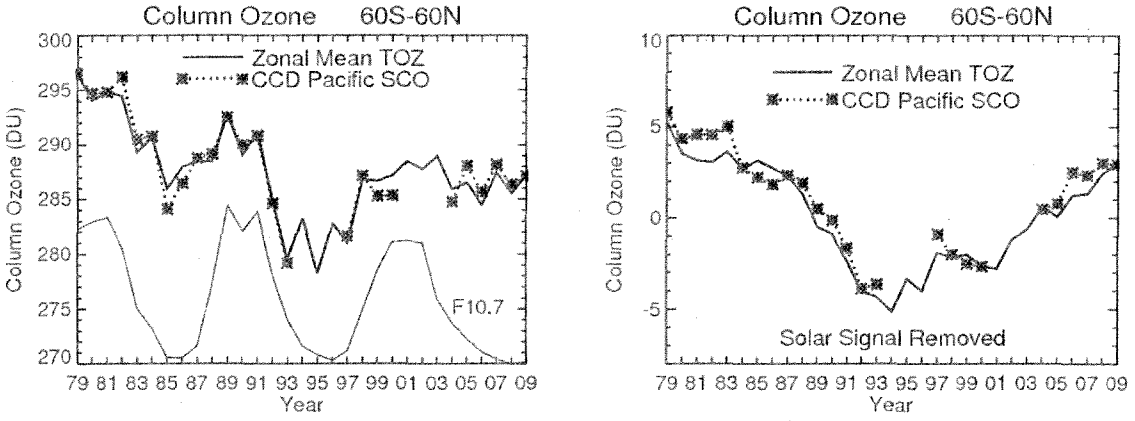

Figure 16. (Left) Annual mean time series of TOMS/SBUV/OMI merged total column ozone (thick solid curve along top), TOMS+OMI CCD measurements of stratospheric column ozone (thick dotted curve along top), and solar F10.7 cm radio flux (thin solid curve along bottom) which has been rescaled for plotting. Stratospheric column ozone has had 31 Dobson Units added for visualization in plotting with total column ozone. Both ozone time series represent area-weighted measurements lying between latitudes 60°S and 60°N. (Right) Similar to ozone plotted in the left panel except that time averages have been removed and the 11-year solar-cycle signals in the two ozone time series have been extracted by linear regression. The regression model used to remove 11-year solar cycle variability in the two ozone time series is (t is year index): $Ozone(t) = C \cdot Solar(t) + \varepsilon(t)$ where C and is a constant, *Solar* is solar F10.7 cm annual mean time series (with time average removed) and ε = model residual error. (The two derived residual series $\varepsilon(t)$ are plotted in the right panel.) A 3-year running average was applied to both time series in the right panel for smoothing.

6. Summary and Conclusions.

The convective-cloud differential (CCD) method is the most basic form of the "cloud slicing" technique. This method generates gridded measurements of TCO and SCO in the tropics and also Pacific mean and zonal mean TCO and SCO extending to high latitudes. The CCD method is assessed using Aura OMI and MLS ozone measurements for the period October 2004 through July 2010. TCO and SCO from the CCD method are compared with corresponding OMI/MLS residual measurements in which MLS ozone profiles are used to calculate SCO. The Aura OMI/MLS data provide greatly improved temporal and spatial coverage for evaluating the CCD measurements as previous validation efforts involved sparse data from SAGE and HALOE (for SCO) and ozonesondes (for TCO).

The analyses indicate that the CCD and OMI/MLS gridded TCO products in the tropics agree to within one DU offset with a mean RMS difference of about 3 DU. RMS differences between these two datasets for inter-annual variations in the Pacific are about 0.5-2.5 DU for either TCO or SCO over most latitudes ranging from the tropics to high latitudes. (RMS differences for TCO are the same as for SCO since total column ozone from OMI is used for both residual methods.) RMS differences for either zonal mean TCO or zonal mean SCO vary from about 0.5-1 DU in the tropics to ~1.5 DU at mid-to-high latitudes.

The Aura OMI/MLS ozone data have given us greater confidence in the CCD measurements of tropospheric and stratospheric ozone derived from previous TOMS measurements. This is important for extending the TOMS data with more recent OMI data to develop a long record of tropospheric and stratospheric ozone for evaluating decadal changes. We have developed from TOMS and OMI measurements a long 32-year (1979-2010) dataset of tropospheric and stratospheric ozone. The analyses of these time series show that the quasi-biennial oscillation (QBO) is the dominant source of inter-annual variability of stratospheric ozone. During the Aura record the QBO variability in stratospheric ozone was of a 24-month periodicity and was clearest throughout the Southern Hemisphere extending to high latitudes. Both CCD and MLS measurements show QBO-related inter-annual variability of stratospheric ozone in the Southern Hemisphere of 30-40 DU. The 32-year dataset also indicates a QBO signal in tropospheric ozone with peak-to-peak amplitudes varying from about 2 DU up to 7 DU. These results further strengthen evidence of a QBO signal in tropospheric ozone as suggested in previous studies based upon much shorter time record measurements from SHADOZ ozonesondes and TOMS satellite ozone.

Trend analysis of the 32-year record dataset suggests a turnaround in global stratospheric column ozone loss in the mid-1990's with current ozone levels comparable to the mid-1980's. The analysis suggests that most of this turnaround occurred in the Northern Hemisphere extending from the subtropics to high latitudes. The trend results are generally consistent with the prediction of past and recent chemistry-climate models which include the reduction of ozone destroying substances beginning in the late 1980's mandated by the Montreal Protocol.

Acknowledgments. The authors thank the Aura MLS and OMI instrument and algorithm teams for the extensive satellite measurements used in this study. We also want to thank S. M. Frith and R. D. Stolarski for providing the merged total ozone data set used in our analyses. OMI is a Dutch-Finnish contribution to the Aura mission. Funding for this research was provided in part by NASA NNH07ZDA001N-AST.

References

Andrews, D. G., J. R. Holton, and C. B. Leovy, *Middle Atmosphere Dynamics*, 489 pp., Academic, San Diego, Calif., 1987.

Chandra, S., J. R. Ziemke, P. K. Bhartia, and R. V. Martin, Tropical tropospheric ozone: Implications for dynamics and biomass burning, *J. Geophys. Res., 107*(D14), doi:10.1029/2001JD00044, 2002.

Chandra, S., J. R. Ziemke, and R. V. Martin, Tropospheric ozone at tropical and middle latitudes derived from TOMS/MLS residual: Comparison with a global model, *J. Geophys. Res., 108*(D9) doi:10.1029/2002JD002912, 2003.

Fishman, J., and J. C. Larsen, Distribution of total ozone and stratospheric ozone in the tropics: Implications for the distribution of tropospheric ozone, *J. Geophys. Res., 92*, 6627-6634, 1987.

Fishman, J., C. E. Watson, J. C. Larsen, and J. A. Logan, Distribution of tropospheric ozone determined from satellite data, *J. Geophys. Res., 95*, 3599-3617, 1990.

Froidevaux, L., Y. B. Jiang, A. Lambert, N. J. Livesey, W. G. Read, J. W. Waters, E. V. Browell, J. W. Hair, M. A. Avery, T. J. McGee, L. W. Twigg, G. K. Sumnicht, K. W. Jucks, J. J. Margitan, B. Sen, R. A. Stachnik, G. C. Toon, P.F. Bernath, C.D. Boone, K.A. Walker, M.J. Filipiak, R.S. Harwood, R.A. Fuller, G. L. Manney, M. J. Schwartz, W. H. Daffer, B. J. Drouin, R. E. Cofield, D. T. Cuddy, R. F. Jarnot, B. W. Knosp, V. S. Perun, W. V. Snyder, P. C. Stek, R. P. Thurstans, and P. A. Wagner, Validation of Aura Microwave Limb Sounder stratospheric ozone measurements," *J. Geophys. Res. 113*, D15S20, doi:10.1029/2007JD008771, 2008.

Folkins, I., C. Braun, A. M. Thompson, and J. C. Witte, Tropical ozone as an indicator of deep convection, J. Geophys. Res., 107(D13), doi:10.1029/2001JD001178, 2002.

Jackman, C. H., E. L. Fleming, S. Chandra, D. B. Considine, and J. E. Rosenfield, Past, present, and future modeled ozone trends with comparisons to observed trends, *J. Geophys. Res., 101*(D22), 28,753-28,767, 1996.

779 Kley, D., P. J. Crutzen, H. G. J. Smit, H. Vomel, S. J. Oltmans, H. Grassl, and V.
780 Ramanathan, Observations of near-zero ozone concentrations over the convective Pacific:
781 Effects on air chemistry, *Science, 274*, 230-232, 1996.
782
783 Lee, S., D. M. Shelow, A. M. Thompson, and S. K. Miller, QBO and ENSO variability in
784 temperature and ozone from SHADOZ, 1998-2005, *J. Geophys. Res., 115*, D18105,
785 doi:10.1029/2009JD013320, 2010.
786
787 Levelt, P. F., E. Hilsenrath, G. W. Leppelmeier, G. H. J. van den Oord, P. K. Bhartia, J.
788 Tamminen, J. F. de Haan, J. P. Veefkind, Science objectives of the Ozone Monitoring
789 Instrument, *IEEE Trans. Geophys. Remote Sens. 44*(5), 1199-1208, 2006.
790
791 Oman, L. D., D. A., Plummer, D. W. Waugh, J. Austin, J. F. Scinocca, A. R. Douglass, R.
792 J. Salawitch, T. Canty, H. Akiyoshi, S. Bekki, P. Braesicke, N. Butchart, M. P.
793 Chipperfield, D. Cugnet, S. Dhomse, V. Eyring, S. Frith, S. C. Hardiman, D. E. Kinnison,
794 J.F. Lamarque, E. Mancini, M. Marchand, M. Michou, O. Morgenstern, T. Nakamura, J.
795 E. Nielsen, D. Olivie, G. Pitari, J. Pyle, E. Rozanov, T. G. Shepherd, K. Shibata, R. S.
796 Stolarski, H. Teyssedre, W. Tian, Y. Yamashita, and J. R. Ziemke, Multi-model
797 assessment of the factors driving stratospheric ozone evolution over the 21st century, *J.*
798 *Geophys. Res., 115*, D24306, doi:10.1029/2010JD014362, 2010.
799
800 Sauvage, B., R. V. Martin, A. van Donkelaar, and J. R. Ziemke, Quantification of the
801 factors controlling tropical tropospheric ozone and the South Atlantic maximum, J.
802 *Geophys. Res., 112*(D11), D11309, doi:1029/2006JD008008, 2007.
803
804 Schoeberl, M. R., A. R. Douglass, E. Hilsenrath, P. K. Bhartia, J. Barnett, R. Beer, J.
805 Waters, M. Gunson, L. Froidevaux, J. Gille, P. F. Levelt, and P. DeCola, Overview of the
806 EOS Aura Mission, *IEEE Trans. Geosci. Remote Sensing 44*(5), 1066-1074, May 2006.
807
808 Schoeberl, M. R., J. R. Ziemke, B. Bojkov, N. Livesey, B. Duncan, S. Strahan, L.
809 Froidevaux, S. Kulawik, P. K. Bhartia, S. Chandra, P. F. Levelt, J. C. Witte, A. M.
810 Thompson, E. Cuevas, A. Redondas, D. W. Tarasick, J. Davies, G. Bodeker, G. Hansen,
811 B. J. Johnson, S. J. Oltmans, H. Vomel, M. Allaart, H. Kelder, M. Newchurch, S. Godin-
812 Beekmann, G. Ancellet, H. Claude, S. B. Andersen, E. Kyro, M. Parrondos, M. Yela, G.
813 Zablocki, D. Moore, H. Dier, P. von der Gathen, P. Viatte, R. Stubi, B. Calpini, P.
814 Skrivankova, V. Dorokhov, H. De Backer, F. J. Schmidlin, G. Coetzee, M. Fujiwara, V.
815 Thouret, F. Posny, G. Morris, J. Merrill, C. P. Leong, G. Koenig-Langlo, and E. Joseph,
816 A trajectory-based estimate of the tropospheric ozone column using the residual method,
817 *J. Geophys. Res., 112*, D24S49, doi:10.1029/2007JD008773, 2007.
818
819 Solomon, S., D. W. J. Thompson, R. W. Portmann, S. J. Oltmans, and A. M. Thompson,
820 On the distribution and variability of ozone in the tropical upper troposphere:
821 Implications for tropical deep convection and chemical-dynamical coupling, *Geophys.*
822 *Res. Lett., 32*, L23813, doi:10.1029/2005GL024323, 2005.
823

824 Steinbrecht, W., U. Kohler, H. Claude, M. Weber, J. P. Burrows, and R. J. van der A,
825 Very high ozone columns at northern mid-latitudes in 2010, *Geophys. Res. Lett., 38*,
826 L06803, doi:10.1029/2010GL046634, 2011.
827
828 Vomel, H., and K. Diaz, Ozone sonde cell current measurements and implications for
829 observations of near-zero ozone concentrations in the tropical upper troposphere, Atmos.
830 Meas. Tech., 3, 495-505, doi:10.5194/amt-3-495-2010, 2010.
831
832 Waters, J.W., L. Froidevaux, R.S. Harwood, R.F. Jarnot, H.M. Pickett, W.G. Read, P.H.
833 Siegel, R.E. Cofield, M.J. Filipiak, D.A. Flower, J.R. Holden, G.K. Lau, N.J. Livesey,
834 G.L. Manney, H.C. Pumphrey, M.L. Santee, D.L. Wu, D.T. Cuddy, R.R. Lay, M.S. Loo,
835 V.S. Perun, M.J. Schwartz, P.C. Stek, R.P. Thurstans, M.A. Boyles, S. Chandra, M.C.
836 Chavez, G-S. Chen, B.V. Chudasama, R. Dodge, R.A. Fuller, M.A. Girard, J.H. Jiang, Y.
837 Jiang, B.W. Knosp, R.C. LaBelle, J.C. Lam, K.A. Lee, D. Miller, J.E. Oswald, N.C. Patel,
838 D.M. Pukala, O. Quintero, D.M. Scaff, W.V. Snyder, M.C. Tope, P.A. Wagner, and M.J.
839 Walch, The Earth Observing System Microwave Limb Sounder (EOS MLS) on the Aura
840 satellite, *IEEE Trans. Geosci. Rem. Sens. 44*(5), 2006.
841
842 WMO (World Meteorological Organization) *Scientific assessment of ozone depletion:*
843 *2010*, Global Ozone Research and Monitoring Project-Report No. 52, Geneva,
844 Switzerland, 2011.
845
846 Ziemke, J. R., S. Chandra, and P. K. Bhartia, Two new methods for deriving tropospheric
847 column ozone from TOMS measurements: The assimilated UARS MLS/HALOE and
848 convective-cloud differential techniques, *J. Geophys. Res., 103*, 22,115-22,127, 1998.
849
850 Ziemke, J. R., and S. Chandra, Seasonal and inter-annual variabilities in tropical
851 tropospheric ozone, *J. Geophys. Res., 104*, 21,425-21,442, 1999.
852
853 Ziemke, J. R., S. Chandra, and P. K. Bhartia, "Cloud slicing": A new technique to derive
854 upper tropospheric ozone from satellite measurements, *J. Geophys. Res., 106*, 9853-9867,
855 2001.
856
857 Ziemke, J. R., S. Chandra, and P. K. Bhartia, A 25-year data record of atmospheric ozone
858 from TOMS Cloud Slicing: Implications for trends in stratospheric and tropospheric
859 ozone, *J. Geophys. Res., 110*, D15105, doi:10.1029/2004JD005687, 2005.
860
861 Ziemke, J. R., S. Chandra, B. N. Duncan, L. Froidevaux, P. K. Bhartia, P. F. Levelt, and J.
862 W. Waters, Tropospheric ozone determined from Aura OMI and MLS: Evaluation of
863 measurements and comparison with the Global Modeling Initiative's Chemical Transport
864 Model, *J. Geophys. Res., 111*, D19303, doi:10.1029/2006JD007089, 2006.
865
866 Ziemke, J. R., J. Joiner, S. Chandra, P. K. Bhartia, A. Vasilkov, D. P. Haffner, K. Yang,
867 M. R. Schoeberl, L. Froidevaux, and P. F. Levelt, Ozone mixing ratios inside tropical
868 deep convective clouds from OMI satellite measurements, *Atmos. Chem. Phys., 9*, 573-
869 583, 2009.